Asymptotic Analysis of Plane Wave Scattering by a Fast Moving PEC Wedge

Ram Tuvi and Timor Melamed, *Senior Member, IEEE*

***Abstract*— This contribution is concerned with the exact and asymptotic scattering of an oblique incident time-harmonic electromagnetic plane wave from a fast moving perfectly electric conducting wedge. By utilizing the Lorentz transformation and applying Maxwell's boundary conditions in the (scatterer) co-moving frame, an exact solution for the total fields is obtained in both the co-moving (scatterer) and the laboratory (incident field) frames. The fields are evaluated asymptotically in the high frequency regime in which the scattered field is presented as a sum of three wave types: the direct (reflected) wave, a shadowing wave, and a diffraction wave. Novel relativistic wave phenomena that are associated with the scatterer dynamics are explored.**

***Index Terms*— Asymptotic analysis, special relativity, wedge diffraction.**

I. Introduction

THE subject of electromagnetic (EM) field scattering from uniformly moving objects is a significant discipline due to its numerous applications in different fields such as communication, RADAR, and object recognition. By obtaining solutions to canonical problems, a generalization for approximated models can be made in order to address the more generic and complex scatterers. Such canonical problem is the scattering from a moving perfectly electric conductor (PEC) half-plane and PEC wedge.

Various solutions for diffraction of plane waves (PWs) by a *stationary* wedge are explored in the literature. By applying eigenfunction and integral representation the exact fields were obtained in [1]. Asymptotic solutions were derived in [2] for a wedge with an angle which is less than π. In [3] and [4], a high frequency solutions were obtained, which are valid only outside the shadow and reflection boundaries (transition regions). A uniform asymptotic solutions were derived in [5] and [6], where the dyadic diffraction coefficients were obtained in the form of Fresnel integrals.

In many situations of practical importance, engineers and physicists deal with scattering of EM waves from *moving* objects (see [7]). The case of a PW normally incident on a moving PEC flat plate (half-plane) was considered in [8]. Exact, as well as, uniform quasi-stationary approximated solutions were constructed from the wave profile of the scattered field. This problem was further investigated in [9], where the effect of the motion on the reflection and shadow zones, aberration, Doppler shift, edge-diffracted wave, etc., was explored and parameterized. In [10], the problem of EM wave scattering by a PEC wedge in uniform translating motion is treated by means of a PW spectra representation approach. The exact analytical solution was compared with two different numerical techniques. The scattering of an EM PW from moving PEC half-plane and PEC wedge was investigated in [11]–[13]. These investigations were conducted for the 2-D case and do not include several 3-D wave phenomena. Other recent contributions to relativistic scattering can be found in [14]–[20].

The canonical problem of EM scattering from wedges has gained a large intention in the literature due to its significant theoretical and practical importance. Its asymptotic analysis that reveals unique wave phenomena is considered as a milestone in wave theory. Nevertheless, to the best of the authors' knowledge, a complete 3-D asymptotic analysis of *moving* wedge scattering has not yet been carried out. Such analysis reveals novel wave phenomena such as the impact of the wedge velocity on the structure of Keller's cone, shifts in the reflection/shadow boundaries, and so on. The analysis is used in order to adjust canonical local interaction field models to the scatterer movement. On the practical side, the resulting models can serve for characterizing communication channels where the antenna or the environment is moving such as urban environment and indoor communication. The present canonical problem of EM PW scattering can be extended for a wider class of problems, such as Gaussian beam scattering, using PW spectral decomposition of the incident field.

II. Problem Definition

In the present contribution, we address the exact and the asymptotic scattering solution for the fast moving wedge and discuss the relativistic wave phenomena that are associated with the scatterer dynamics. In order to address the problem of PW scattering from a wedge that is translating uniformly, we consider here two inertial frames of reference, the *incident-wave frame* and the co-moving *scatterer frame* that is translating uniformly with respect to the incident-wave frame. According to Einstein's Special Relativity, an event (x, y, z, ct) in the incident-wave frame is mapped to an event (x', y', z', ct') in the scatterer frame via the Lorentz transformation (LT) [7]

$$x' = \gamma (x - vt), \quad y' = y, \quad z' = z, \quad ct' = \gamma (ct - \beta x) \quad (1)$$

where, in the present investigation, we assume that the scatterer's velocity is

$$\mathbf{v} = v\hat{\mathbf{x}} \quad (2)$$

Manuscript received November 30, 2016; revised March 31, 2017; accepted April 20, 2017. Date of publication May 2, 2017; date of current version July 1, 2017. *(Corresponding author: Timor Melamed.)*

The authors are with the Department of Electrical and Computer Engineering, Ben-Gurion University of the Negev, Beer-Sheva 84105, Israel.

Color versions of one or more of the figures in this paper are available online at http://ieeexplore.ieee.org.

Digital Object Identifier 10.1109/TAP.2017.2700165

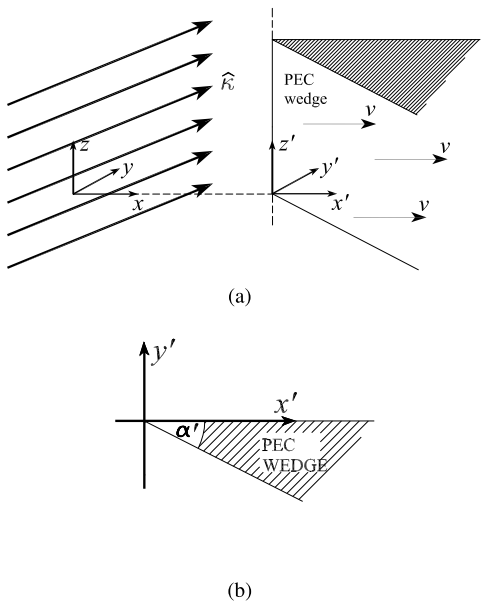

Fig. 1. Physical configuration. (a) Time-harmonic PW is impinging on a PEC wedge that is translating with a speed of v in the direction of the x-axis. The scatterer co-moving frame is denoted by (x', y', z'). (b) Scattering object is a PEC wedge with a α' head angle in the scatterer co-moving frame.

with $\hat{\mathbf{x}}$ denoting the unit vector in the direction of the x-axis. In (1), $c = 1/\sqrt{\varepsilon_0 \mu_0}$ denotes the speed of light in vacuum, and

$$\gamma = 1/\sqrt{1-\beta^2}, \quad \beta = v/c. \tag{3}$$

Quantities in the scatterer frame are denoted by a prime.

According to Special Relativity, the EM *field transformation* (FT) that is corresponding to the velocity in (2) is given by [7]

$$\begin{aligned} E'_x &= E_x, \quad E'_y = \gamma\,(E_y - v\mu_0 H_z), \quad E'_z = \gamma\,(E_z + v\mu_0 H_y) \\ H'_x &= H_x, \quad H'_y = \gamma\,(H_y + v\epsilon_0 E_z), \quad H'_z = \gamma\,(H_z - v\epsilon_0 E_y) \end{aligned} \tag{4}$$

where β and γ are given in (3). The corresponding *inverse* LT (ILT) and the *inverse* FT (IFT) are obtained by interchanging all primed and un-primed quantities in (1) and (4), and replacing v with $-v$.

We consider the scattering of the time-harmonic PW that is given by

$$\begin{aligned} \mathbf{E}^i(\mathbf{r}, t) &= \mathbf{E}_0 \exp\left[j\left(\omega t - k\hat{\boldsymbol{\kappa}}^i \cdot \mathbf{r}\right)\right] \\ \mathbf{H}^i(\mathbf{r}, t) &= \mathbf{H}_0 \exp\left[j\left(\omega t - k\hat{\boldsymbol{\kappa}}^i \cdot \mathbf{r}\right)\right] \end{aligned} \tag{5}$$

where $k = \omega/c$ denotes the wavenumber and

$$\hat{\boldsymbol{\kappa}}^i = \left(\kappa_x^i, \kappa_y^i, \kappa_z^i\right) = (-\cos\phi_0 \sin\theta_0, -\sin\phi_0 \sin\theta_0, \cos\theta_0) \tag{6}$$

is a unit vector in the direction of propagation of the PW as in Fig. 1(a). Anticipating the use of the LT in (1), we have kept the time dependence of $\exp(j\omega t)$ explicitly in (5).

The PW in (5) is impinging on a PEC wedge that is translating uniformly in vacuum. The wedge velocity is given by (2) [see Fig. 1(a)]. The wedge is infinite in the z-direction, with a head angle of $\alpha' < \pi$ [see Fig. 1(b)]. This angle is measured in the scatterer co-moving frame. In the scatterer frame, where the wedge is stationary, the boundary conditions of the PEC surfaces are given by

$$\hat{\mathbf{n}}' \times \mathbf{E}' = 0, \ \hat{\mathbf{n}}' \cdot \mathbf{B}' = 0 \tag{7}$$

where $\hat{\mathbf{n}}' = \hat{\mathbf{y}}$ over the $\phi' = 0$ upper surface, and $\hat{\mathbf{n}}' = -\hat{\boldsymbol{\phi}}' = -\sin\alpha'\hat{\mathbf{x}} - \cos\alpha'\hat{\mathbf{y}}$ over the $\phi' = (2\pi - \alpha')$ lower surface. Here ϕ' denotes the conventional cylindrical coordinate in the scatterer frame.

III. EM Fields in the Scatterer Co-Moving Frame

By applying the transformations in (1), (4), to (5), we obtain the *incident* PW in the scatterer frame in the form

$$\begin{aligned} \mathbf{E}^{i\prime}(\mathbf{r}', t') &= \mathbf{E}'_0 \exp\left[j\left(\omega' t' - k'\hat{\boldsymbol{\kappa}}'^i \cdot \mathbf{r}'\right)\right] \\ \mathbf{H}^{i\prime}(\mathbf{r}', t') &= \mathbf{H}'_0 \exp\left[j\left(\omega' t' - k'\hat{\boldsymbol{\kappa}}'^i \cdot \mathbf{r}'\right)\right]. \end{aligned} \tag{8}$$

Here,

$$\mathbf{E}'_0 = \begin{bmatrix} E_{0_x} \\ \gamma\,(E_{0_y} - v\mu_0 H_{0_z}) \\ \gamma\,(E_{0_z} + v\mu_0 H_{0_y}) \end{bmatrix}, \quad \mathbf{H}'_0 = \begin{bmatrix} H_{0_x} \\ \gamma\,(H_{0_y} + v\epsilon_0 E_{0_z}) \\ \gamma\,(H_{0_z} - v\epsilon_0 E_{0_y}) \end{bmatrix} \tag{9}$$

γ is given in (3)

$$\omega' = \gamma\,\omega\left(1 - \kappa_x^i \beta\right), \quad k' = \gamma\, k\left(1 - \kappa_x^i \beta\right) \tag{10}$$

and

$$\hat{\boldsymbol{\kappa}}'^i = \left[\gamma\left(\kappa_x^i - \beta\right), \kappa_y^i, \kappa_z^i\right] / \left[\gamma\left(1 - \kappa_x^i \beta\right)\right]. \tag{11}$$

The scatterer frame spherical angles of the incident PW unit vector $\hat{\boldsymbol{\kappa}}'^i$ in (11) can be expressed directly by the incident-wave frame $\hat{\boldsymbol{\kappa}}^i$ components via

$$\begin{aligned} \cos\theta'_0 &= \kappa_z^i / \gamma\left(1 - \kappa_x^i \beta\right) \\ \cos\phi'_0 &= -\left(\kappa_x^i - \beta\right) / \left[\left(\kappa_x^i - \beta\right)^2 + \kappa_y^{i\,2} \gamma^{-2}\right]^{1/2}. \end{aligned} \tag{12}$$

In view of (8), the scattering problem in the scatterer frame is reduced to a PW diffraction by a *stationary* wedge (with the corresponding frequency and wavenumber).

The exact and asymptotic solutions for the total EM field due to a PW diffraction by a *stationary* wedge are well known [6], [21]. The procedure applies the two Hertz potentials, Ψ'_A and Ψ'_F, that are corresponding to either the electric (TM) or the magnetic (TE) z-components of the incident PW, respectively. The EM fields are derived from the potentials by applying the differential operators in [6].

Following [6], the total field potentials in the scatterer frame that are corresponding to the incident field in (8) are given by

$$\begin{aligned} \Psi'_A(\mathbf{r}', t') &= \Psi'_{A_0} g'_s\left(\rho', \phi'; \phi'_0, \theta'_0\right) \exp\left(j\omega' t' - jk' z' \cos\theta'_0\right) \\ \Psi'_F(\mathbf{r}', t') &= \Psi'_{F_0} g'_h\left(\rho', \phi'; \phi'_0, \theta'_0\right) \exp\left(j\omega' t' - jk' z' \cos\theta'_0\right) \end{aligned} \tag{13}$$

where (ρ', ϕ') are the conventional cylindrical coordinates in the scatterer frame and

$$\begin{aligned} \Psi'_{A_0} &= j\omega'\varepsilon_0 \left(k' \sin\theta'_0\right)^{-2} E'_{0z} \\ \Psi'_{F_0} &= j\omega'\mu_0 \left(k' \sin\theta'_0\right)^{-2} H'_{0z}. \end{aligned} \tag{14}$$

Here k' and ω' are given in (10), $\hat{\boldsymbol{\kappa}}'^{i}$ is given in (11), and E'_{0z} and H'_{0z} are given in (9).

The TM (soft) and TE (hard) wedge Green's functions (GFs) that are denoted by $g'_{s,h}$ are given by

$$g'_{s,h}(\rho',\phi';\phi'_0,\theta'_0) = g'(\rho',\phi';\phi'_0,\theta'_0) \mp g'(\rho',\phi';-\phi'_0,\theta'_0) \tag{15}$$

with $0 < \phi' < N'\pi$ and $g'(\rho',\phi';\phi'_0,\theta'_0)$ is given by the integral representation in [6]. In (15), the $\mp$ signs correspond to either the TM or TE GFs.

Next, we discuss the *asymptotic* form of the GFs in (15), for the special case $\alpha' < \pi$. Following the formulations in [6] and [21], the asymptotic TM and TE GFs in (15) consist of geometrical optics (GO) GFs and diffraction GFs, that is

$$g'_{s,h}(\rho',\phi';\phi'_0,\theta'_0) \sim g'^{GO}_{s,h}(\rho',\phi';\phi'_0,\theta'_0) + g'^{d}_{s,h}(\rho',\phi';\phi'_0,\theta'_0). \tag{16}$$

The explicit expressions for the TE or TM EM asymptotic fields are obtained by applying the differential operators in [6] to (13) with (16) and collecting the higher order k'-terms.

The GO GFs, $g'^{GO}_{s,h}$, are given by

$$\begin{aligned} &g'^{GO}_{s,h}(\rho',\phi';\phi'_0,\theta'_0) \\ &= U(\pi-|\Phi'^{-}|)\exp\left[jk'\rho'\sin\theta'_0\cos(\Phi'^{-})\right] \\ &\quad \mp U(\pi-|\Phi'^{+}|)\exp\left[jk'\rho'\sin\theta'_0\cos(\Phi'^{+})\right] \\ &\quad \mp U(\pi-|2\pi N'-\Phi'^{+}|)\exp\left[jk'\rho'\sin\theta'_0\cos(2\pi N'-\Phi'^{+})\right] \end{aligned} \tag{17}$$

where

$$N' = (2\pi - \alpha')/\pi. \tag{18}$$

$U(t)$ denotes the (Heaviside) unit step function, the $\mp$ signs proceeding the Heaviside functions correspond to either the TM or the TE polarizations, respectively, and Φ'^{+} and Φ'^{-} are given by

$$\Phi'^{\mp} = \phi' \mp \phi'_0. \tag{19}$$

Using (17) in (13), we identify the first term in (17) as the *incident* PW potential. The second term is identified as the *reflected* PW from the surface $\phi' = 0$ and the third term as the *reflected* PW from the lower $\phi' = N'\pi$ surface.

In (16), $g'^{d}_{s,h}$ denotes the soft or hard diffraction GFs

$$\begin{aligned} g'^{d}_{s,h}(\rho',\phi';\phi'_0,\theta'_0) &= \sqrt{\sin\theta'_0}\,D'_{s,h}(\phi';\phi'_0,\theta'_0) \\ &\quad \times \frac{\exp\left(-jk'\rho'\sin\theta'_0\right)}{\sqrt{\rho'}} \end{aligned} \tag{20}$$

where $D_{s,h}$ denotes the uniform (soft or hard) diffraction coefficients that are given by

$$\begin{aligned} &D'_{s,h}(\phi';\phi'_0,\theta'_0) \\ &= \left(\sin\theta'_0\right)^{-1}\Big\{d^{+}(\Phi'^{-})F\left[k'\rho'\sin\theta'_0 a^{+}(\Phi'^{-})\right] \\ &\qquad + d^{-}(\Phi'^{-})F\left[k'\rho'\sin\theta'_0 a^{-}(\Phi'^{-})\right] \\ &\qquad \mp d^{+}(\Phi'^{+})F\left[k'\rho'\sin\theta'_0 a^{+}(\Phi'^{+})\right] \\ &\qquad \mp d^{-}(\Phi'^{+})F\left[k'\rho'\sin\theta'_0 a^{-}(\Phi'^{+})\right]\Big\}. \end{aligned} \tag{21}$$

Here,

$$F(x) = 2j|\sqrt{x}|\exp(jx)\int_{|\sqrt{x}|}^{\infty}\exp(-j\tau^2)d\tau \tag{22}$$

denotes the transition function, and

$$\begin{aligned} d^{\pm}(\Phi') &= -\frac{1}{2N'}\frac{\exp(-j\pi/4)}{\sqrt{2\pi k'}}\cot\left(\frac{\pi \pm \Phi'}{2N'}\right) \\ a^{\pm}(\Phi') &= 2\cos^2\left(\frac{2N'\pi n'^{\pm} - \Phi'}{2}\right) \end{aligned} \tag{23}$$

with $n'^{\pm}$ is an integer which mostly satisfies the condition

$$n'^{\pm} = (\mp\pi + \Phi')/(2\pi N'). \tag{24}$$

The integral in (22) is identified as the Fresnel integral.

The diffraction GFs in (20) are in the standard GTD form [4] in which the incident PW is sampled at the edge point $x' = 0, y' = 0$, and multiplied by the UTD diffraction coefficient. The phase term in (13) with (20) is in the form of a diffraction cone with a head angle of θ'. Note that unlike the GTD diffraction coefficients, the UTD diffraction coefficients are continuous over the illumination and reflection boundaries. For $k'r'\sin\theta'_0 \gg 10$, one can replace $F(x) \to 1$, and the UTD and GTD diffraction coefficients converge [21].

IV. EM Fields in the Incident-Field Frame

A. Exact Solution

The exact fields in the incident-field frame are obtained in the following procedure: first, we derive the EM fields in the *scatterer* frame in cylindrical coordinate. Next, we present the scatterer frame EM fields in a cartesian coordinates using

$$\hat{\boldsymbol{\rho}}' = \cos\phi'\hat{\mathbf{x}} + \sin\phi'\hat{\mathbf{y}}, \quad \hat{\boldsymbol{\phi}}' = -\sin\phi'\hat{\mathbf{x}} + \cos\phi'\hat{\mathbf{y}}. \tag{25}$$

Finally, by applying the IFT and the ILT, we obtain the EM fields in the the incident-field frame from the potentials in (13). This procedure yields

$$\begin{aligned} \mathbf{E}(\mathbf{r},t) &= \mathbf{E}_A(\mathbf{r},t) + \mathbf{E}_F(\mathbf{r},t) \\ \mathbf{H}(\mathbf{r},t) &= \mathbf{H}_A(\mathbf{r},t) + \mathbf{H}_F(\mathbf{r},t) \end{aligned} \tag{26}$$

where

$$\begin{aligned} \mathbf{E}_{A,F}(\mathbf{r},t) &= \mathbf{L}_E(\mathbf{r},t)\left[\boldsymbol{\mathcal{D}}'_{A,F}\Psi'_{A,F}(\mathbf{r}',t')\right]\Big|_{\substack{r'(\mathbf{r},t)\\ t'(\mathbf{r},t)}} \\ \mathbf{H}_{A,F}(\mathbf{r},t) &= \mathbf{L}_H(\mathbf{r},t)\left[\boldsymbol{\mathcal{D}}'_{A,F}\Psi'_{A,F}(\mathbf{r}',t')\right]\Big|_{\substack{r'(\mathbf{r},t)\\ t'(\mathbf{r},t)}}. \end{aligned} \tag{27}$$

Here,

$$\begin{aligned} &\mathbf{L}_E(\mathbf{r},t) \\ &= \begin{bmatrix} C(t) & -S(t) & 0 & 0 & 0 & 0 \\ \gamma S(t) & \gamma C(t) & 0 & 0 & 0 & \Upsilon_\mu \\ 0 & 0 & \gamma & -\Upsilon_\mu S(t) & -\Upsilon_\mu C(t) & 0 \end{bmatrix} \\ &\mathbf{L}_H(\mathbf{r},t) \\ &= \begin{bmatrix} 0 & 0 & 0 & C(t) & S(t) & 0 \\ 0 & 0 & -\Upsilon_\varepsilon & \gamma S(t) & \gamma C(t) & 0 \\ \Upsilon_\varepsilon S(t) & \Upsilon_\varepsilon C(t) & 0 & 0 & 0 & \gamma \end{bmatrix} \end{aligned} \tag{28}$$

where $\Upsilon_\mu = \gamma\upsilon\mu_0$, $\Upsilon_\varepsilon = \gamma\upsilon\varepsilon_0$, and $S(t) = \sin\phi(t)$, $C(t) = \cos\phi(t)$, with

$$\phi(t) = \tan^{-1}\left[\frac{y}{\gamma\,(x-\upsilon t)}\right]. \tag{29}$$

In (27),

$$\mathcal{D}'_A = \begin{bmatrix} -\cos\theta'_0\eta_0\partial_{\rho'} \\ -\cos\theta'_0\rho'^{-1}\eta_0\partial_{\phi'} \\ \left(k'\sin\theta'_0\right)^2(j\omega'\varepsilon_0)^{-1} \\ \rho'^{-1}\partial_{\phi'} \\ -\partial_{\rho'} \\ 0 \end{bmatrix}$$

$$\mathcal{D}'_F = \begin{bmatrix} -\rho'^{-1}\partial_{\phi'} \\ \partial_{\rho'} \\ 0 \\ -\cos\theta'_0\eta_0^{-1}\partial_{\rho'} \\ -\cos\theta'_0(\eta_0\rho')^{-1}\partial_{\phi'} \\ \left(k'\sin\theta'_0\right)^2(j\omega'\mu_0)^{-1} \end{bmatrix} \tag{30}$$

where $\eta_0 = (\mu_0/\varepsilon_0)^{1/2}$ is the free space impedance. The EM fields in (27) are obtained by applying the differential operators $\mathcal{D}'_{A,F}$ to the scatterer-frame Hertz potentials in (13) and then sampling at the corresponding incident-wave frame event in (1). Alternatively, by inserting $\mathcal{D}'_{A,F}$ in (30) into (27) and using the LT in (1), this operation can be recast in the form

$$\begin{aligned} \mathbf{E}_{A,F}(\mathbf{r},t) &= \mathbf{L}_E(\mathbf{r},t)\mathcal{D}_{A,F}\Psi_{A,F}(\mathbf{r},t) \\ \mathbf{H}_{A,F}(\mathbf{r},t) &= \mathbf{L}_H(\mathbf{r},t)\mathcal{D}_{A,F}\Psi_{A,F}(\mathbf{r},t). \end{aligned} \tag{31}$$

In this representation, the EM fields are obtained by applying differential operators *directly* in the incident-field frame. To that extent, we define two incident-field frame potentials that are denoted by $\Psi_{A,F}(\mathbf{r},t)$. These potentials are obtained by sampling the scatterer frame Hertz potentials at the corresponding incident-wave frame event according to the LT in (1), that is

$$\Psi_{A,F}(\mathbf{r},t) = \Psi'_{A,F}(\mathbf{r}',t')\Big|_{\begin{cases} r'(\mathbf{r},\mathbf{t}) \\ \mathbf{t}'(\mathbf{r},\mathbf{t}) \end{cases}}. \tag{32}$$

The differential operators $\mathcal{D}_{A,F}(\mathbf{r},t)$ in (31) are obtained by replacing in (30) the partial derivations, $\partial_{\rho'}$ and $\partial_{\phi'}$, with

$$\begin{aligned} \partial_{\rho'} &= \gamma\cos\phi'\partial_x + \sin\phi'\partial_y + \gamma\cos\phi'\beta c^{-1}\partial_t, \\ \partial_{\phi'} &= -\gamma\rho'\sin\phi'\partial_x + \rho'\cos\phi'\partial_y - \gamma\beta\rho'\sin\phi' c^{-1}\partial_t \end{aligned} \tag{33}$$

and then replacing ϕ' with $\phi(t)$ in (29) and ρ' with

$$\rho(t) = \sqrt{\gamma^2(x-vt)^2 + y^2}. \tag{34}$$

Note that the $\psi_{A,F}(\mathbf{r},t)$ potentials in (32) are *not* the conventional Hertz potentials so that the derivation of the EM fields from $\psi_{A,F}(\mathbf{r},t)$ is carried out via (31) (and not by applying the standard operators in [6]).

Next, we evaluate the *asymptotic* scattered potentials in (32). By inserting (16) into (13) and applying the ILT, the asymptotic incident-field frame potentials, $\Psi_A(r,t)$ and $\Psi_F(r,t)$, are recast in the form

$$\Psi_{A,F}(\mathbf{r},t) = \Psi^{\mathrm{GO}}_{A,F}(\mathbf{r},t) + \Psi^{d}_{A,F}(\mathbf{r},t). \tag{35}$$

The GO and the diffraction potentials are defined and discussed in Sections IV-B and IV-C, respectively. Note the solution is valid for $0 < \phi(t) < N'\pi$, i.e., outside the scatterer, and for $(\kappa_x^{i\,2} + \kappa_y^{i\,2})^{1/2}k\rho(t) \gg 1$ where $\rho(t)$ is given in (34).

B. GO Potentials

Following the discussion after (19), the GO potentials in (35) are composed of the incident PW, $\Psi^i_{A,F}$, and of the reflected PWs from the upper and lower surfaces, which are denoted by $\Psi^{ru}_{A,F}$ and $\Psi^{rl}_{A,F}$, respectively. Thus

$$\Psi^{\mathrm{GO}}_{A,F}(\mathbf{r},t) = \Psi^i_{A,F}(\mathbf{r},t) + \Psi^{ru}_{A,F}(\mathbf{r},t) + \Psi^{rl}_{A,F}(\mathbf{r},t) \tag{36}$$

where

$$\begin{aligned} \Psi^i_{A,F}(\mathbf{r},t) &= \Psi'_{A_0,F_0}U\left(\pi - \left|\phi(t) - \phi'_0\right|\right)\exp\left[-jk\Omega^{\mathrm{GO}}_i(\mathbf{r},t)\right] \\ \Psi^{ru}_{A,F}(\mathbf{r},t) &= \mp\Psi'_{A_0,F_0}U\left(\pi - \left|\phi(t) + \phi'_0\right|\right)\exp\left[-jk\Omega^{\mathrm{GO}}_{ru}(\mathbf{r},t)\right] \\ \Psi^{rl}_{A,F}(\mathbf{r},t) &= \mp\Psi'_{A_0,F_0}U\left\{\pi - \left|2\pi N' - \left[\phi(t) + \phi'_0\right]\right|\right\} \\ &\quad\times\exp\left[-jk\Omega^{\mathrm{GO}}_{rl}(\mathbf{r},t)\right]. \end{aligned} \tag{37}$$

Here $\phi(t)$ is given in (29) and N' is given in (18), Ψ'_{A_0,F_0} are given in (14), and the GO phases are given by

$$\begin{aligned} &\Omega^{\mathrm{GO}}_i(\mathbf{r},t) = \hat{\boldsymbol{\kappa}}^i\cdot\mathbf{r} - ct, \quad \Omega^{\mathrm{GO}}_{ru}(\mathbf{r},t) = \hat{\boldsymbol{\kappa}}^{ru}\cdot\mathbf{r} - ct \\ &\Omega^{\mathrm{GO}}_{rl}(\mathbf{r},t) = \mathbf{s}\cdot\mathbf{r} - ct\gamma^2\left[1 - \kappa^i_x\beta + \beta\left(\gamma\cos 2\alpha'\left(\kappa^i_x - \beta\right)\right.\right. \\ &\qquad\left.\left. - \sin 2\alpha'\kappa^i_y\right)/\gamma\right] \end{aligned} \tag{38}$$

where $\hat{\boldsymbol{\kappa}}^i$ is the incident PW normalized wavenumber in (6), $\hat{\boldsymbol{\kappa}}^{ru} = (\kappa^i_x, -\kappa^i_y, \kappa^i_z)$ and the vector $\mathbf{s} = (s_x, s_y, \kappa^i_z)$ with

$$\begin{aligned} s_x &= \gamma^2\cos 2\alpha'\left(\kappa^i_x - \beta\right) - \gamma\sin 2\alpha'\kappa^i_y + \gamma^2\beta\left(1 - \kappa^i_x\beta\right) \\ s_y &= -\sin 2\alpha'\gamma\left(\kappa^i_x - \beta\right) - \cos 2\alpha'\kappa^i_y. \end{aligned} \tag{39}$$

These vectors are identified as the PWs directions of propagation of the corresponding potentials in the incident-wave frame.

The incident and upper surface reflection potentials *phase terms* are identical to the stationary scatterer phases in [21]. These potentials differ from the stationary scatterer ones only in the Heaviside functions arguments in (37), which restrict the contributions to the time-dependent shadow and reflection regions. For the *stationary* scatterer, the shadow boundary is given by $y = \tan\phi_0 x$ and the reflection boundaries are given by $y = -\tan\phi_0 x$ for the upper surface, and

$$y = \frac{-\sin\theta_0\cos\phi_0\tan 2\alpha' - \sin\theta_0\sin\phi_0}{\sin\theta_0\cos\phi_0 - \tan 2\alpha'\sin\theta_0\sin\phi_0}x \tag{40}$$

for the lower one. Here ϕ_0 and θ_0 denotes the conventional spherical angles that are associated with the incident PW unit vector in (6), namely

$$\hat{\boldsymbol{\kappa}}^i = (-\sin\theta_0\cos\phi_0, -\sin\theta_0\sin\phi_0, \cos\theta_0). \tag{41}$$

Note that unlike the stationary case, the moving wedge shadow and reflection boundaries are not parallel to the incident and reflected PWs direction of propagation, respectively (similar to the phenomenon in [9]). The time dependent *shadow* boundary is obtained by setting to zero the Heaviside function argument of $\Psi^i_{A,F}$ in (37), giving

$$\phi(t) - \phi'_0 = \pm\pi. \tag{42}$$

Using (12) and (29) in (42), this condition reads [see more details after (49)]

$$y = \frac{\sin\theta_0\sin\phi_0}{\sin\theta_0\cos\phi_0 + \beta}(x - vt). \tag{43}$$

In a similar manner, the lower surface *reflection* boundary is given by

$$y = -\frac{\sin\theta_0 \sin\phi_0}{\sin\theta_0 \cos\phi_0 + \beta}(x - \upsilon t). \tag{44}$$

For the special case of normal incidence, $\theta_0 = \pi/2$, these results agrees with those in [9].

The time dependence of the reflection boundaries are due to the (incident-field frame) time dependent boundary conditions. The boundary conditions in the scatterer frame are given in (7). By applying the ILT and IFT to (7), the corresponding *incident-field frame* boundary conditions of the upper PEC surface take the form

$$\begin{aligned} &E_x = H_y = 0 \quad \text{at } y = 0, \quad x > \upsilon t \\ &E_z = 0 \quad \text{at } y = 0, \quad x > \upsilon t. \end{aligned} \tag{45}$$

These conditions are similar to the stationary wedge with the exception of the $x = \upsilon t$ time-dependent location of the wedge's edge. This is a special case where the normal to the surface has no components in the direction of the surface velocity $\mathbf{v}$ [see (48)].

Next, we examine the reflected potential and the reflection boundary of the *lower* surface in (44). By comparing the phase term of lower surface reflected potentials, $\Psi^{rl}_{A,F}(\mathbf{r}, t)$, to the phase term of the upper surface reflected potential, $\Psi^{ru}_{A,F}(\mathbf{r}, t)$, in (38) we note that unlike the upper surface reflection, the reflected potentials from the *lower* surface exhibits a frequency scaling of $\omega\gamma^2[1-\kappa^i_x\beta+\beta(\gamma\cos 2\alpha'(\kappa^i_x-\beta)-\sin 2\alpha'\kappa^i_y)/\gamma]$. The scaling is a result of the wedge velocity component *normal* to the surface.

In the scatterer frame, the wedge angle is α' and the *lower surface* satisfies $\phi' = N'\pi$, i.e., $y' = -x'\tan\alpha'$. Using the ILT this surface in the incident-field frame is given by

$$y = -(x - \upsilon t)\tan\alpha, \quad \tan\alpha = \gamma\tan\alpha'. \tag{46}$$

Here α is identified as the incident-field frame *head angle*. The normal unit vector to the lower surface is given by

$$\hat{\mathbf{n}} = -(\sin\alpha, \cos\alpha, 0). \tag{47}$$

Note that both the normal and the head angle are velocity dependent.

In the *incident-field frame* the boundary conditions are given by [7, Chap. 5, Eqs. (5.3) and (5.5)]

$$\hat{\mathbf{n}}\cdot\mathbf{B} = 0, \quad \hat{\mathbf{n}}\times\mathbf{E} - (\hat{\mathbf{n}}\cdot\mathbf{v})\mathbf{B} = 0. \tag{48}$$

Similar to the upper surface, the lower surface reflection boundary is not parallel to the reflected ray that impinges on the edge at the origin at time t. The reflection boundary from the lower surface, which is obtained by setting the argument of the Heaviside function in (36) to zero, is given by

$$y = \frac{-\gamma(\sin\theta_0\cos\phi_0 + \beta)\tan 2\alpha' - \sin\theta_0\sin\phi_0}{\gamma(\sin\theta_0\cos\phi_0 + \beta) - \tan 2\alpha'\sin\theta_0\sin\phi_0}\gamma(x - \upsilon t). \tag{49}$$

Next, we examine the shift of the lower surface reflection boundary in (49) from the stationary case one. For simplicity, we examine the special case of $\kappa^i_z = 0$ (i.e., $\theta_0 = \pi/2$).

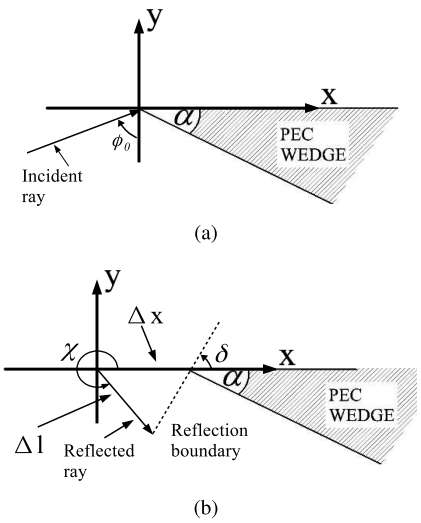

Fig. 2. Reflection boundary of the lower surface of the moving wedge in (49). (a) At time $t = 0$, the incident ray is impinging near the edge of the wedge and generates a reflected wavefront. (b) At time $t > 0$, the wedge's edge is located at the point $x = \upsilon t$. The straight line that connects the edge and the reflected ray wavefront forms the reflection boundary.

To that end, we track an incident ray trajectory (wavefront). We assume that the ray is impinging near the edge of the wedge at time $t = 0$ as illustrated in Fig. 2(a). This ray reflects from the lower surface in the direction of χ [see Fig. 2(b)]. Using the notations in (39)

$$\tan\chi = s_y/s_x. \tag{50}$$

At time $t > 0$, the reflected ray travels a distance of ct while the wedge travels a distance of υt as illustrated in Fig. 2(b). The straight line that connects the edge of the wedge and the reflected wave font forms the reflection boundary. Referring to Fig. 2(b) and using the sine theorem, $\Delta_l/\sin\delta = -\Delta_x/\sin(\chi-\delta)$. By setting $\Delta_l = ct$ and $\Delta_x = \upsilon t$ we obtain

$$\tan\delta = \sin\chi/(\cos\chi - \beta). \tag{51}$$

Finally, by substituting (50) into (51) and using (39), we obtain the reflection boundary in (49).

C. Diffraction Potentials

The diffraction potentials in (35) are given by

$$\begin{aligned} \Psi^d_{A,F}(\mathbf{r}, t) = {} & \Psi'_{A_0,F_0}\sqrt{\sin\theta'_0}D_{s,h}\big[\phi(t); \phi'_0, \theta'_0\big] \\ & \times \frac{\exp(-j\pi/4)}{\sqrt{\rho(t)}}\exp(-jk\Omega^d) \end{aligned} \tag{52}$$

where Ψ'_{A_0,F_0} are given in (14), ϕ'_0 and θ'_0 are given in (12), $\phi(t)$ is given in (29), $\rho(t)$ is given in (34), and the diffraction phase term is given by

$$\begin{aligned} \Omega^d = {} & \sqrt{\gamma^2(\kappa^i_x - \beta)^2 + \kappa^{i\,2}_y}\,\rho(t) + \kappa^i_z z \\ & + \gamma^2(1 - \kappa^i_x\beta)(\beta x - ct). \end{aligned} \tag{53}$$

In (52), $D_{s,h}$ denotes the soft or hard incident-wave frame diffraction coefficients

$$\begin{aligned} &D_{s,h}\left[\phi(t);\phi_0',\theta_0'\right] \\ &= \left(\sin\theta_0'\right)^{-1}\left\{d^+[\Phi^-(t)]F\left[k'\sin\theta_0'\rho(t)a^+(\Phi^-(t))\right]\right. \\ &\quad + d^-[\Phi^-(t)]F\left[k'\sin\theta_0'\rho(t)a^-(\Phi^-(t))\right] \\ &\quad \mp d^+[\Phi^+(t)]F\left[k'\sin\theta_0'\rho(t)a^+(\Phi^+(t))\right] \\ &\quad \left.\mp d^-[\Phi^+(t)]F\left[k'\sin\theta_0'\rho;a^-(\Phi^+(t))\right]\right\} \quad (54) \end{aligned}$$

where $d^{\pm}()$ and $a^{\pm}()$ are given in (23), F is given in (22), and

$$\Phi^{\mp}(t) = \phi(t) \mp \phi_0'. \quad (55)$$

Next, we examine the relativistic analog of Keller's diffraction cone. Using (53), the surfaces of constant phase, $\Omega^d = \Omega_0^d$ are given by

$$\begin{aligned} \sqrt{\gamma^2\left(\kappa_x^i-\beta\right)^2+\kappa_y^{i2}}\rho(t) &= \Omega_0^d - \kappa_z^i z \\ &\quad + \gamma^2\left(1-\kappa_x^i\beta\right)(ct-\beta x). \quad (56) \end{aligned}$$

Referring to the diffraction potentials in (52), we note that unlike in the stationary case, the phase term for the *moving* wedge is not a (ρ-) cylindrical wave. Next by dividing (56) by $\gamma\left(1-\kappa_x^i\beta\right)$ and inserting (12), we obtain

$$\sin\theta_0'\rho(t) = C(z) - \cos\theta_0' z + \gamma\left(ct-\beta x\right) \quad (57)$$

where

$$C(z) = \left[\gamma\left(1-\kappa_x^i\beta\right)\right]^{-1}\Omega_0^d - \cos\theta_0' z. \quad (58)$$

Finally, by inserting $\rho(t)$ in (34) into (57), we recast (56) in the form

$$\begin{aligned} &\gamma^2(\sin^2\theta_0'-\beta^2)x^2 - 2x\left[\sin^2\theta_0'\gamma^2\beta ct - \gamma\beta C(z) - \gamma^2\beta ct\right] \\ &\quad + \sin^2\theta_0' y^2 - D(z,t) = 0 \quad (59) \end{aligned}$$

where

$$D(z,t) = C^2(z) + 2C(z)\gamma ct + (\gamma ct)^2 - \left(\gamma\sin\theta_0'\beta ct\right)^2. \quad (60)$$

Equation (59) is in the form of a conic equation. Its cross sections over constant z-planes depend on the velocity and the angle of incidence. For $\kappa_z^i = 0$ the cross sections are circular as shown in [13]. For $\kappa_t' > \beta$, (59) describes elliptical cross sections, and for $\kappa_t' \le \beta$ the cross sections are hyperbolas.

V. Simulations

First we plot in Fig. 3 the diffraction surfaces of constant phase (wave fronts) in (59) for the two diffraction regimes in which κ_t' is either larger or smaller than β. In Fig. 3(a) we set $\beta = 0.8$, $\theta_0 = \pi/4$, and $\phi_0 = 5\pi/3$. The corresponding *elliptical* cross sections over constant z-planes are plotted in Fig. 3(b). By setting $\beta = 0.9$, $\theta_0 = \pi/4$, and $\phi_0 = 4\pi/3$ we obtain the wavefront and its *hyperbolic* cross sections in Fig. 3(c) and (d), respectively. The arrows in Fig. 3(a) and (c) are local directions of the wavefront propagation. These arrows form the dynamic version of Keller's cone.

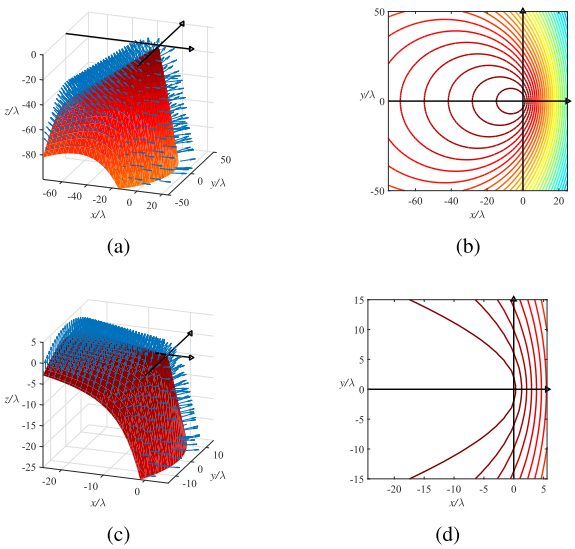

Fig. 3. The diffraction surfaces of constant phase in (59). (a) Surface for $\upsilon = 0.8c$, $\theta_0 = \pi/4$, and $\phi_0 = 5\pi/3$ and (b) its ellipsoidal contours over constant z-planes, (c) Surface for $\upsilon = 0.9c$, $\theta_0 = \pi/4$, and $\phi_0 = 4\pi/3$ and (d) its hyperbolic contours over constant z-planes.

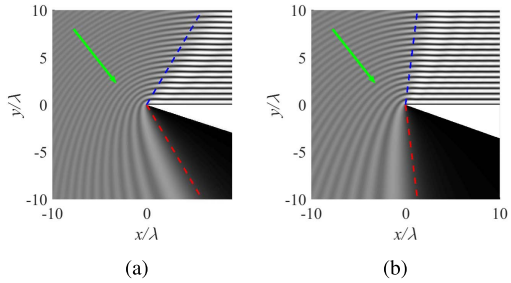

Fig. 4. Shifts of the reflection and shadow boundaries. The total electric potential and the boundaries for (a) stationary wedge and (b) moving wedge with $\beta = 0.4$.

In order to demonstrate the shifts of the reflection and shadow boundaries, we plot the total asymptotic potential amplitude at time $t = 0$ for stationary and moving wedges in Fig. 4(a) and (b), respectively. In both figures the TM polarized incident field is impinging from the direction $\phi_0 = 2/3\pi$, $\theta_0 = 0$ and the wedge (scatterer frame) angle is $\alpha' = \pi/10$. For these parameters, the field is reflected only from the upper surface. The asymptotic potential is evaluated using the uniform diffraction coefficients in (54). In Fig. 4(b), the wedge is moving in $\upsilon = 0.4c$. Note the difference of the reflection (blue line) and shadow (red line) boundaries between the stationary and moving cases according to (43) and (44).

Finally, in Fig. 5 we plot the amplitude of the asymptotic electric potential as a function of time at two observation points, above ($y = 10\lambda$) and below ($y = -10\lambda$) the moving wedge in Fig. 5(a) and (b), respectively. In both figures $x = 0$. The wedge parameters are $\alpha' = \pi/6$ and $\beta = 0.4$. The incident PW is as in Fig. 3. The uniform asymptotic potential is plotted versus the normalized time $\upsilon t/\lambda$. Note that the field is not a time-harmonic one. Thus the amplitude of the asymptotic electric potential is the time-dependent (slowly varying) envelope of the rapidly oscillating potential.

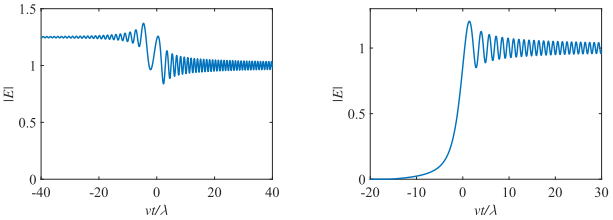

Fig. 5. Total electric potential's amplitude as a function of time at two observation points (a) above and (b) below the moving wedge.

For the observation point above the wedge in Fig. 5(a), the *reflection* boundary in (44) is passing through the observation point at time $vt_r/\lambda = -1.26$. Thus, for time $t \ll t_r$, the main contribution for the potential arises from the incident and reflected potentials resulting in the constant amplitude that is clearly viewed in the figure. For time $t \gg t_r$, the observation point is away from the transition region and the total potential consists of mainly the incident potential resulting in a constant amplitude. The potential in the transition region (about $t = t_r$) has a time dependent amplitude due to the contribution of the diffraction term in (52).

For the observation point below the wedge in Fig. 5(b), the observation point is located inside the PEC for time $vt/\lambda < -15.87$. The *shadow* boundary in (43) is passing through the observation point at time $vt_s/\lambda = -1.26$. Thus for time $t \ll t_s$ the observation point is located inside the wedge or deep into the shadow region which results in the null potential in the figure. For time $t \gg t_s$ the observation point is away from the transition region and the total potential mainly consists of the incident potential resulting in a constant amplitude. The potential in the transition region (about $t = t_s$) has a time dependent amplitude due to the contribution of the diffraction term in (52).

VI. Conclusion

In this paper several novel wave phenomena that are associated with PW scattering from a moving PEC wedge were presented and explored, in order to gain insights regarding the effect of the scatterer dynamics on the scattering mechanism and on the field's canonical forms. Furthermore, the incident PW serve as the basis wave propagators for a generic EM incident wave. Thus the solutions that are presented here, can be applied for obtaining the scattered fields for different waveobjects such as Gaussian beams and GFs.

References

[1] H. M. Macdonald, *Electric Waves*. Cambridge, U.K.: Cambridge Univ. Press, 1902.
[2] W. Pauli, "On asymptotic series for functions in the theory of diffraction of light," *Phys. Rev.*, vol. 54, no. 11, pp. 924–931, 1938.
[3] A. Sommerfeld, "Asymptotische darstellung von formeln aus der beugungstheorie des lichtes," *J. Reine Angewandte Math.*, vol. 158, no. 4, pp. 199–208, 1927.
[4] J. B. Keller, "Geometrical theory of diffraction," *J. Opt. Soc. Amer.*, vol. 52, no. 2, pp. 116–130, 1962.
[5] P. H. Pathak and R. G. Kouyoumjian, "The dyadic diffraction coefficient for a perfectly conducting wedge," Ohio State Univ Columbus Electrosci. Lab, Tech. Rep. TR-2183-4, 1970, pp. 1–87.
[6] R. G. Kouyoumjian and P. H. Pathak, "A uniform geometrical theory of diffraction for an edge in a perfectly conducting surface," *Proc. IEEE*, vol. 62, no. 11, pp. 1448–1461, Nov. 1974.
[7] J. Van Bladel, *Relativity and Engineering*. New York, NY, USA: Springer-Verlag, 1984.
[8] J. Cooper, "Scattering of electromagnetic fields by a moving boundary: The one-dimensional case," *IEEE Trans. Antennas Propag.*, vol. 28, no. 6, pp. 791–795, Nov. 1980.
[9] M. Idemen and A. Alkumru, "Relativistic scattering of a plane-wave by a uniformly moving half-plane," *IEEE Trans. Antennas Propag.*, vol. 54, no. 11, pp. 3429–3440, Nov. 2006.
[10] P. De Cupis, "Diffraction by a moving wedge: Comparison of analytic solution and numerical techniques," in *Proc. 14th Riunione Nazionaledi di Elettromagnetismo*, Ancona, Italy, 2002.
[11] A. Ciarkowski and B. Atamaniuk. (2004). "Electromagnetic diffraction on a moving half-plane." [Online]. Available: https://arxiv.org/abs/math-ph/0412003
[12] A. Ciarkowski, "Electromagetic pulse diffraction by a moving half-plane," *Prog. Electromagn. Res.*, vol. 64, pp. 53–67, 2006.
[13] A. Ciarkowski, "Scattering of an electromagnetic pulse by a moving wedge," *IEEE Trans. Antennas Propag.*, vol. 57, no. 3, pp. 688–693, Mar. 2009.
[14] P. De Cupis, G. Gerosa, and G. Schettini, "Electromagnetic scattering by uniformly moving bodies," *J. Electromagn. Waves Appl.*, vol. 14, no. 8, pp. 1037–1062, 2000.
[15] P. De Cupis, P. Burghignoli, G. Gerosa, and M. Marziale, "Electromagnetic wave scattering by a perfectly conducting wedge in uniform translational motion," *J. Electromagn. Waves Appl.*, vol. 16, no. 3, pp. 345–364, 2002.
[16] P. De Cupis, D. Anatriello, and G. Gerosa, "An asymptotically exact technique for electromagnetic scattering by uniformly moving objects with arbitrary geometry," in *Proc. 27th General Assembly URSI*, 2002, pp. 509–512.
[17] M. Idemen and A. Alkumru, "Influence of the velocity on the energy patterns of moving scatterers," *J. Electromagn. Waves Appl.*, vol. 18, no. 1, pp. 3–22, 2004.
[18] P. De Cupis, "An analytical solution for electromagnetic wave scattering by multiple wedges," *Opt. Commun.*, vol. 261, pp. 203–208, May 2006.
[19] T. Danov and T. Melamed, "Spectral analysis of relativistic dyadic Green's function of a moving dielectric-magnetic medium," *IEEE Trans. Antennas Propag.*, vol. 59, no. 8, pp. 2973–2979, Aug. 2011.
[20] T. Danov and T. Melamed, "Two-dimensional relativistic longitudinal Green's function in the presence of a moving planar dielectricâŁ"magnetic discontinuity," *J. Opt. Soc. Amer. A, Opt. Image Sci.*, vol. 29, no. 3, pp. 285–294, 2011.
[21] G. L. James, *Geometrical Theory of Diffraction for Electromagnetic Waves*. London, U.K.: IEE, 1980.

Ram Tuvi was born in Holon, Israel, in 1982. He received the B.Sc. and M.Sc. (*cum laude*) degrees in electrical and computer engineering from the Ben-Gurion University of the Negev, Beer-Sheva, Israel, in 2010 and 2013, respectively. He is currently pursuing the Ph.D. degree with the Department of Physical-Electronics, School of Electrical Engineering, Tel-Aviv University, Tel-Aviv, Israel.

His current research interests include wave theory, scattering theory, and inverse scattering.

Timor Melamed (SM'94) was born in Tel-Aviv, Israel, in 1964. He received the B.Sc. (*magna cum laude*) degree in electrical engineering and the Ph.D. degree from Tel-Aviv University, Tel-Aviv, in 1989 and 1997, respectively.

From 1996 to 1998, he held a post-doctoral position with the Department of Aerospace and Mechanical Engineering, Boston University, Boston, MA, USA. He is currently with the Department of Electrical and Computer Engineering, Ben-Gurion University of the Negev, Beer-Sheva, Israel. He is a supporter of HTA. His current research interests include analytic techniques in wave theory, transient wave phenomena, inverse scattering, and electrodynamics.